IRAQI BULLETIN OF GEOLOGY AND MINING (IBGM)\
IRAQ GEOLOGICAL SURVEY (GEOSURV-IRAQ)

*IBGM (**2025**, Vol 21; Issue 2)* *129-152*

GEOMETRICAL ANALYSIS OF MINOR FOLDS DEVELOPED IN THE ASHKAWTA RASH AND SARKHOSH ANTICLINES NORTHEAST OF SULAIMANI DISTRICT, IRAQI KURDISTAN REGION

Peshraw S. M. Khalifa[1,*], Salim H. Sulaiman Al-Hakari[1]

[1] Affiliation: Department of Earth Sciences and Petroleum, College of Science, University of Sulaimani, Sulaymaniyah City, Kurdistan Region, Iraq

* Correspondence: Peshraw.mohammedkhalifa@univsul.edu.iq; Peshraw S. M. Khalifa (0009-0007-1453-6630)

Type of the Paper (Article)
Received: 14/02/2025
Accepted: 22/05/2025
Available online: 27/12/2025

Abstract

Fifty-three minor folds within the Ashkawta Rash and Sarkhosh anticlines are studied in detail using various geometric analysis methods. The study area is located about 20 km southeast of Sulaimani City in the Iraqi Kurdistan Region, inside the Zagros Imbricate Zone. The minor folds are located within the Balambo and Kometan formations. The objective of the study is to investigate the relationships between minor and major folds, focusing on their importance in analyzing tectonic development and regional structure, and identifying the processes and mechanisms that contribute to anticline development. Pi (π) diagrams are used to determine the geometric properties of the fold. Fleuty's (1964) classification was used to fold tightness and type, while Ramsey's (1967) framework provided the classification of fold styles, indicating the aspect ratio (h) and normalized area (A) for understanding the asymmetry of single-folded surfaces in minor folds. The analysis of congruous minor folds revealed paleostress orientations of NE – SW. The anticlockwise rotation of the Arabian Plate compared to the Eurasian Plate results in an oblique plate collision related to sub-congruous minor folds. The variations in thickness along fold limbs with varying inclinations of the folded layers indicate a transition in fold geometries from parallel (sub-class 1B) to similar (class 2) types. According to the single-fold surface categorization, the majority of minor folds have a sinusoidal shape, although a few exhibit a chevron shape. The analysis of minor fold geometry indicates that the development of minor folds is mainly influenced by buckling and flattening mechanisms.

Keywords: Buckling mechanism; Congruous minor fold; Homogeneous flattening mechanisms; Parallel fold (sub-class 1B); Sinusoidal shape

1. Introduction

Folds form in both single and multiple rock strata, with sizes varying from microscopic to kilometric. They can occur in any rock type, though they are predominantly observed in

ISSN 1811-4539, EISSN 3005-3714
https://doi.org/10.59150/ibgm2102a08
IBGM: http://ibgm-iq.org/
Academic Scientific Journals: www.iasj.net

extensively deformed rocks inside orogenic zones (Bhattacharya, 2022; Billings, 1974; Ramsay & Huber, 1987). For tectonic studies within orogens, folds are particularly useful because they can be used to determine the directions and rate of tectonic shortening, interpret the geometry of larger-scale structures, analyze the rheological characteristics of the folded rocks, and reveal details about the deformation that occurs to the rocks and their conditions during deformation. (Hudleston & Lan, 1993; Nabavi & Fossen, 2021). Minor folds commonly appear at the hinge regions and along the limbs of larger folds, generally orienting their axes parallel to those of the major fold. The smaller structures are referred to as parasitic folds. In the hinge zone of a substantial fold, these parasitic folds are often symmetrical and are occasionally referred to as M-folds due to their distinct shape. As a result, the parasitic folds located on the limbs of huge folds are often asymmetrical. Based on their profile, they may be designated as Z-folds or S-folds, indicating their distinct shapes (Frehner & Schmid, 2016; Rowland et al., 2007). Fold style refers particularly to a group of morphologic and geometric features that determine the shape of folds (Bastida et al., 2007; Hudleston, 1973). The geometry and shapes of folds provide important information on the deformation type, the shape of deformed layers provides important information on the rheological behavior of rocks, folding mechanisms, and, in situations involving fault-related folds, spatial organization and geometry of the associated fault, and tectonics of a region. Moreover, they have significant economic value, especially as oil reservoirs and in the exploration of ores and mineral resources (Fossen, 2010, 2016; Hudleston, 1973; Lisle et al., 2006). The proposed study aims to analyze the detailed geometric properties, folding styles, and asymmetry of single-folded surfaces of minor folds to determine the relationships between minor and major folds, understanding regional structure, indicating tectonic evolution, and identify the processes and mechanisms that facilitate anticline development.

2. Geological Setting

The Ashkawta Rash and Sarkhosh Anticlines are situated around 20 km southeast of Sulaimani City in the Iraqi Kurdistan Region. The anticlines extend in a northwest-southeast direction following the main direction of the Zagros fold-thrust Belt. They are located between longitudes 45°30'41.07"E and 45°41'52.92"E, and latitudes 35°22'59.24"N and 35°35'6.16"N, as in Figure 1B. Tectonically, Ashkawta Rash and Sarkhosh anticlines are located within the Zagros Imbricate Zone, Figure 1A, which belongs to the Zagros Orogenic Belt and developed along the oblique collision of the Arabian margin with Eurasia (Alavi, 2004). The Balambo Formation, which is Valanginian-Turonian in age, is the oldest rock exposed stratigraphically in the core of the anticlines. Layers of limestone with chert bands, shale, and yellowish-grey marl alternating. This formation is overlain by the Gulneri Shale Formation, which is of Late Cenomanian-Early Turonian age, has a thickness of approximately 2.5 m, and is composed of marly limestone, thin-bedded brown shale, and a high organic matter content. The Kometan Formation, which is Late Turonian to Early Campanian in age, has well-bedded fine-grained limestone with chert bands above the Balambo Formation, as in Figure 2. Overlying the Kometan Formation is the Shiranish Formation, which is Campanian-Maastrichtian in age and is composed of alternating layers of bluish marl and marly limestone.

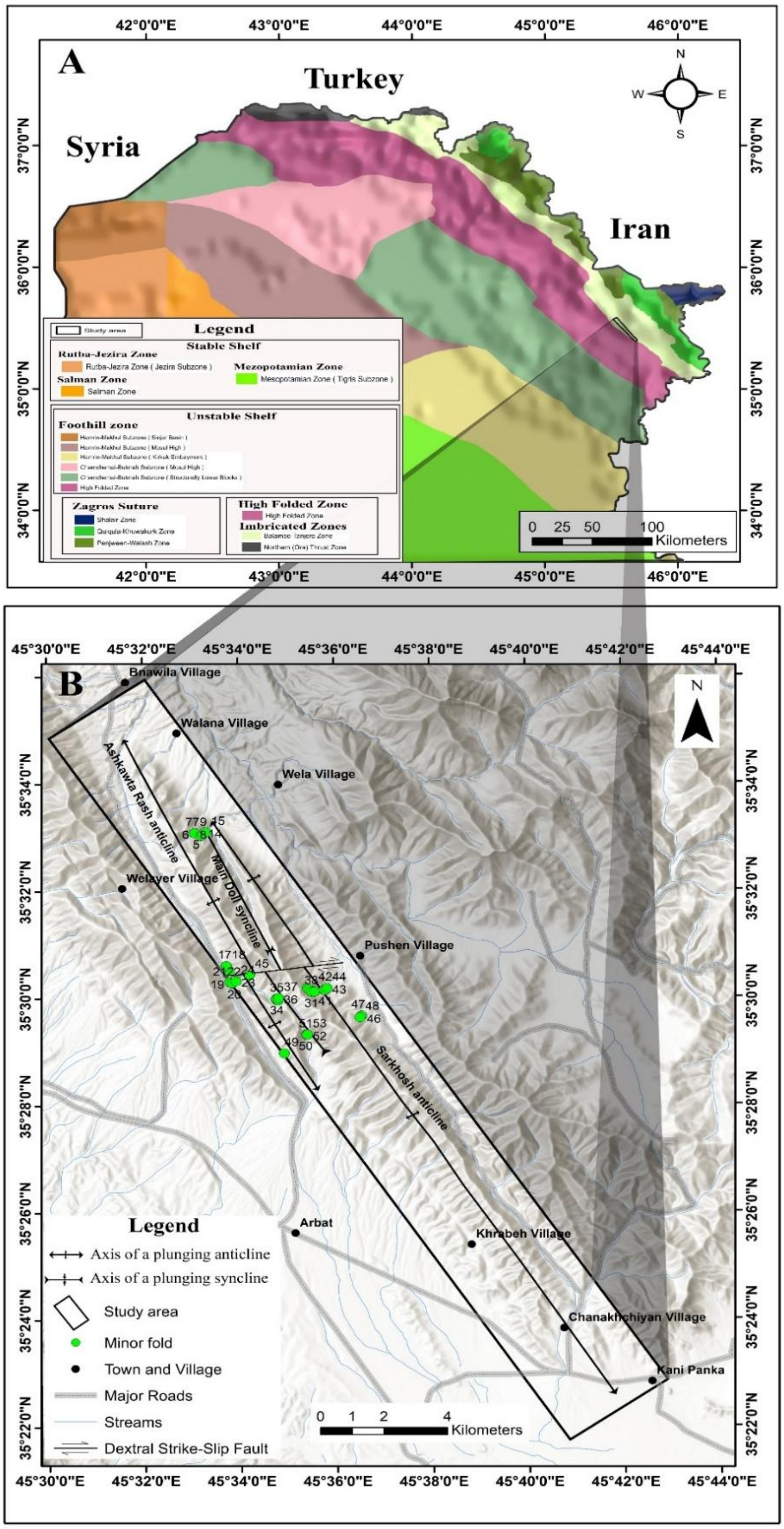

Figure 1. A). The tectonic subdivisions of Iraq (Jassim & Goff, 2006) and B). Location of the study area and geographical distribution of minor folds.

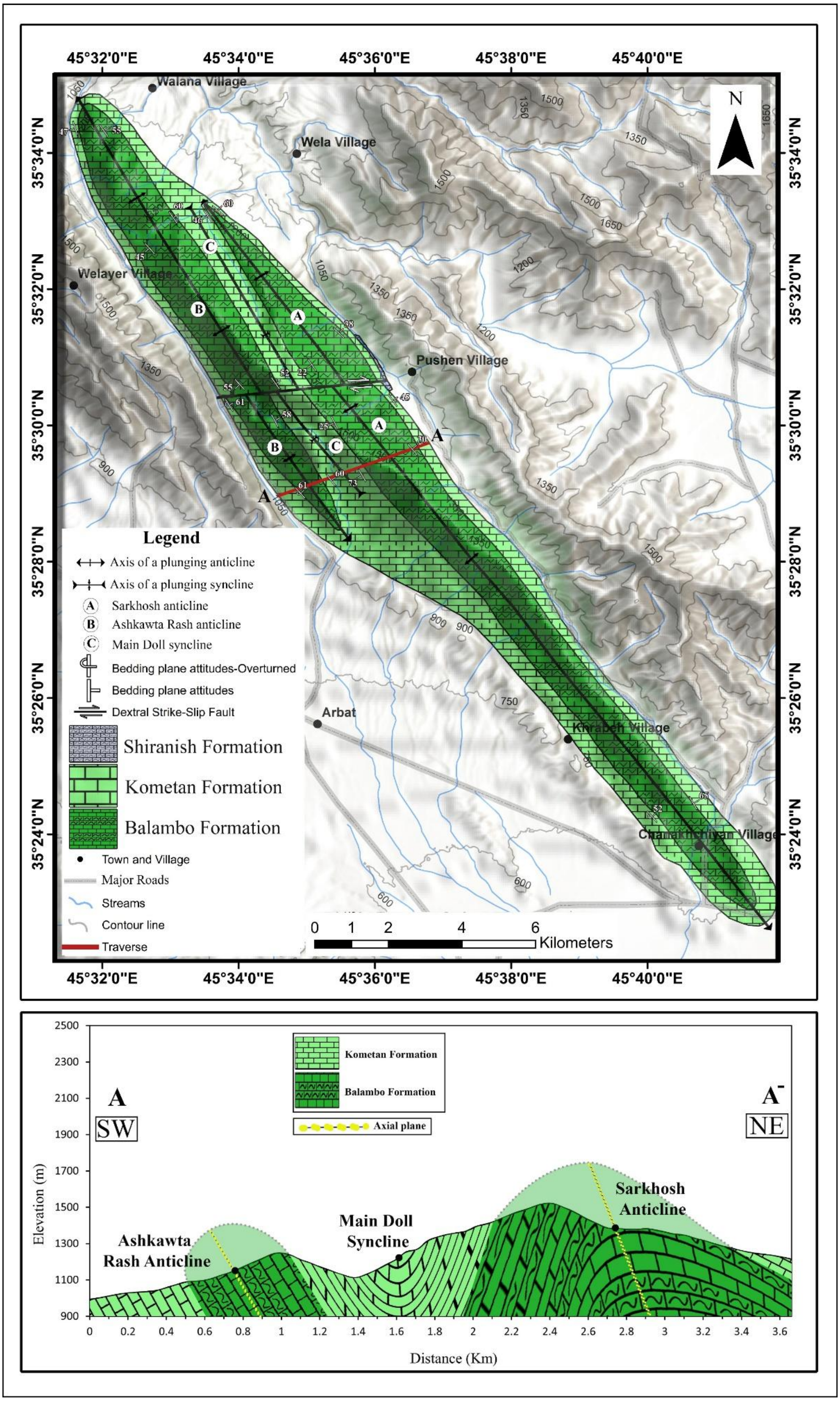

Figure 2. Geological map and geological cross-section along profile (A–A-) of the study area.

3. Methodology

The Right-Hand Rule Right (RHRR) was used to measure the 53 minor folds' orientations. The stereonet program version 11.6.1 (Allmendinger, 2011) was used for drawing the pi (π) diagram to determine essential parameters, such as fold axis and axial plane attitudes, fold vergence and symmetry, interlimb angles, and plunge angles.

The Fleuty classification (Fleuty, 1964) was used to determine fold tightness by the analysis of the interlimb angle and to classify fold types according to the dip of the axial plane and the plunge angle of the hinge.

The folds are classified using Ramsay's 1967 method and are derived from field photos that were taken normal to the fold axis to demonstrate the fold profile. This method depended on a description of the variances in thickness with angle of dip; these measurements are defined as a proportion of the layer thickness at the fold hinge. For folded layers, the elements of style are contained in (dip isogon, orthogonal thickness, and axial trace thickness). According to Ramsay (1967) and Ramsay & Huber (1987), such as tα (orthogonal thickness) or Tα (axial trace thickness) are sufficient for identifying the type of fold class. Only values of tα were used in this study. The ratio of orthogonal thickness (tα) to standard hinge thickness (t_0) is expressed as ($t'_\alpha = t_\alpha/t_0$). The relationship between (t'_α) and dip angle (α) by determining these parameters against one another, illustrating their change with Ramsay diagrams.

According to the classifications in references (Bastida et al., 1999; Bastida et al., 2005), the elements of asymmetric shape folded surfaces are characterized by parameters including the area beneath the limb profile (A), the height (y_0), and the width (x_0) of a limb, which relates to the fold amplitude. The aspect ratio, defined as ($h = y_0/x_0$), and the normalized area, expressed as $A = 2A/x_0y_0$. The relationship between the aspect ratio and the normalized area was examined by graphically representing these variables to explain their variations.

Use ImageJ (1.54g) (Rasband, 1987). software to perform an image analysis of minor folds to determine orthogonal layer thickness (tα), standard hinge thickness (t_0), and the dip angle (α) for dip purpose isogon classification. Additionally, measure the area beneath the limb profile (A), the height (y_0), and the width (x_0) of a limb to asymmetric shape folded surfaces.

4. Results

The Ashkawta Rash and Sarkhosh anticlines along the cross section (A–A-) are represented in Figure 3 as a synoptic stereographic pi (π) diagram. The average attitude of the southwestern (SW) overturned limb of the Ashkawta Rash anticline is 324°/61°, whereas that of the northeastern (NE) limb is 326°/59°. The axial plane's attitude is 325°/61°, whereas the fold axis's attitude is 135°/17°, depending on the Fleuty classification determined by the dip of the axial plane and the plunge of the hinge. Steeply inclined, gently plunging. The interlimb angle is 5°, and the anticline is classified as a tight to inclined isoclinal fold according to Fleuty's classification (Billings, 1974; Fleuty, 1964). A narrow syncline called the Main Doll syncline separates the Ashkawta Rash anticline from the Sarkhosh anticline presented in Figure 2, with the vergency of the anticline heading southwestward. The Sarkhosh anticline's average orientation is 152°/73° for the southwestern limb and 322°/28° for the northeastern limb. The axial plane's attitude is 329°/67°, while the fold axis's attitude is 330°/2°, depending on the dip of the axial plane and the plunge of the hinge, classified as moderately inclined and sub-horizontal. The interlimb angle is 79°, and the anticline is classified as open (Fleuty, 1964).

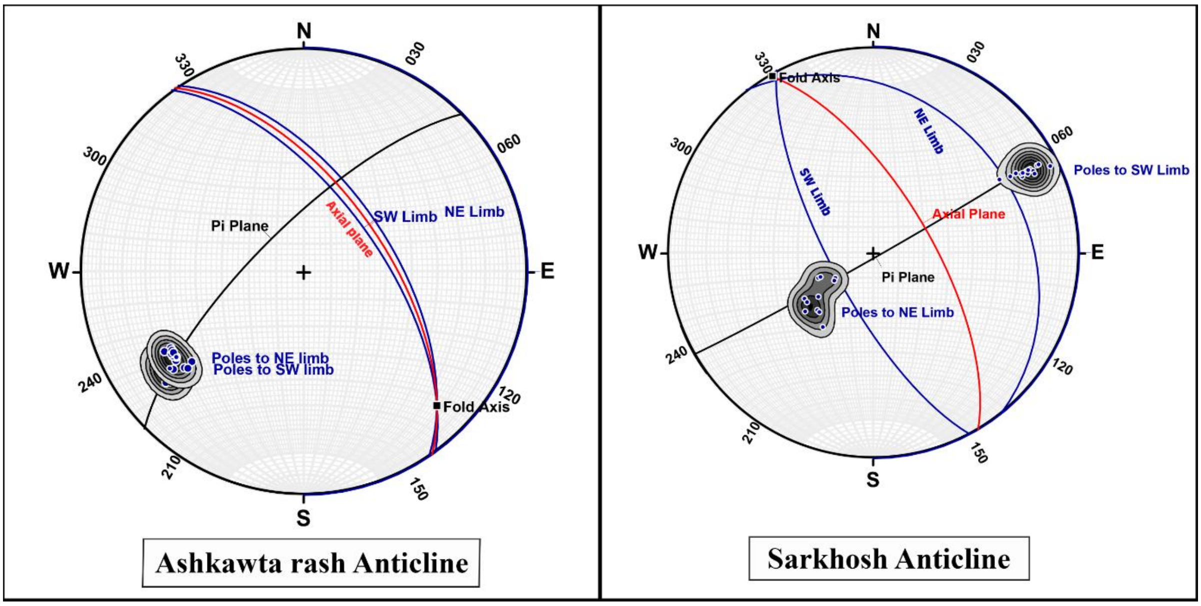

Figure 3. Synoptic stereographic pi (π) diagram of the Ashkawta Rash and Sarkhosh anticlines along cross section (A–A−).

4.1. Geometric Description of a Minor Fold

According to (Fleuty, 1964), the minor folds classify as follows: minor folds numbered 2, 3, 4, 5, 6, 7, 8, 11, 18, 20, 24, 26, 27, 29, 32, 34, 35, 37, 39, 40, 44, 49, 51, and 53 are closed; minor folds numbered 1, 9, 10, 12, 13, 14, 15, 16, 17, 19, 21, 22, 23, 25, 28, 31, 33, 36, 41, 43, 46, 47, 48, 50 and 52 are open; minor folds numbered 30, 38, and 45 are gentle; minor fold numbered 42 is tight, as in Appendix (A) and Figure 4. According to (Fleuty, 1964) depending on the attuite of the axial plane and plunge of the hinge, as in Figure 5 the minor folds are classified as follow: the minor folds numbered 1, 4, 5, 6, 9, 14, 32, 36, 47, 48, 50, 51, and 53 are sub-vertical, sub-horizontal; the minor folds numbered 2, 3, 20, 24, 25, 26, 35, 40, 44, 45, 49, and 52 are sub-vertical, gently plunging; the minor folds numbered 7, 8, 12, 15, 21, 22, 28, 33, 38, and 46 are steeply inclined, sub-horizontal; the minor folds numbered 13, 17, 18, 23, 27, 30, and 37 are steeply inclined, gently plunging; the minor folds numbered 10, 16, and 34 are moderately inclined, sub-horizontal; the minor fold numbered 11 is gently inclined, sub-horizontal; the minor fold numbered 29 is moderately inclined, gently plunging; the minor folds numbered 31, and 43 are vertical, gently plunging, as in Appendix (A).

Figure 4. Minor folds observed in the Ashkawta Rash and Sarkosh anticlines.

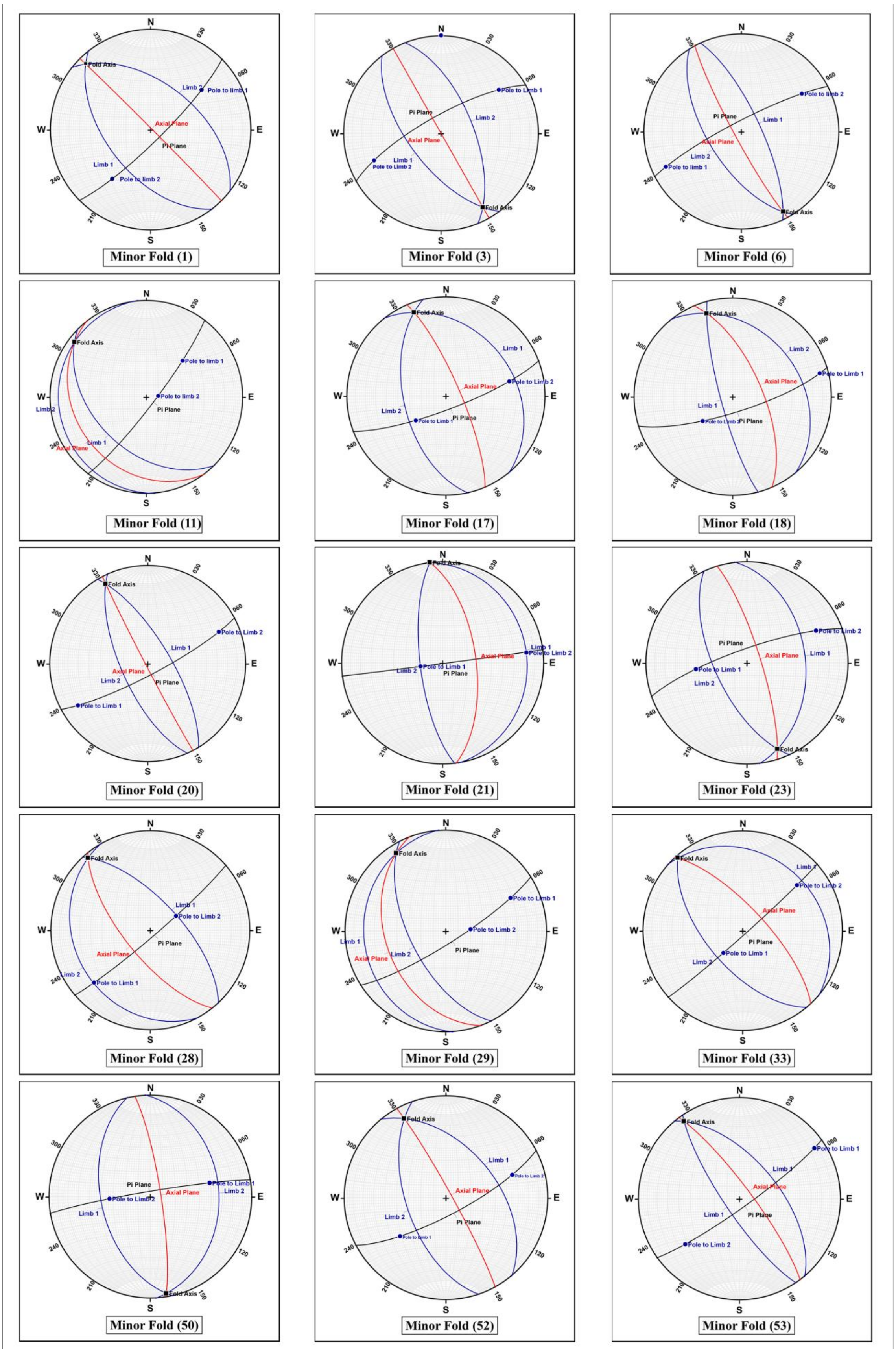

Figure 5. Stereographic projection of some minor folds in the Ashkawta Rash and Sarkosh Anticlines through the Pi (π) diagram.

4.2. Congruous, Sub-Congruous, and Incongruous Minor Folds

When parasitic folds form simultaneously with larger folds, they usually have the same fold axis and axial plane orientations as the primary structure, as explained by Pumpelly's rule (Awais et al., 2016; Frehner & Schmid, 2016). Two classes of minor folds were identified, determined by the association between the major and minor fold axes. Minor folds that are incongruous have axes perpendicular to the axis of the including major anticline, whereas congruous minor folds have axes parallel to the major anticline axis in which they are found. (Billings, 1974; Omar, 2005; Ramsay & Sturt, 1973). This association between congruous and incongruous folding also holds for the relationship between minor and major folds, showing that the same tectonic processes may give the formation of transverse folds (Ramsay & Sturt, 1973). According to Al-Hakari (2023), Al-Hakari (2011), and Majeed (2023), minor folds with axes slightly deviated from the principal fold's axis are termed sub-congruous, indicating their intermediate classification between congruous and incongruous folds. The classification of minor folds in the studied area is determined by the deviation of their axes from the major fold. Minor folds are classified as congruous with deviations ranging from 0° to 12°, sub-congruous from >12° to 60°, and incongruous from >60° to 90°. In the Ashkawta Rash anticline, minor folds numbered as (1, 4, 11, 12, 14, 15, 25, 26, 32, 33, 34, 36, 49, and 53) are congruous, while those numbered (2, 3, 5, 6, 7, 8, 9, 10, 13, 16, 17, 18, 19, 20, 21, 22, 23, 24, 35, 37, 45, 50, 51, and 52) are sub-congruous, as in Appendix (A) and Figure 6A show details. In the Sarkhosh anticline, minor folds numbered (28, 29, 31, 38, 39, 40, 44, 46, 47, and 48) are congruous, but folds numbered (27, 30, 41, 42, and 43) are sub-congruous. No incongruous folds appeared in either the Ashkawta Rash or Sarkhosh anticlines (Appendix A and Figure 6B).

4.3. Fold Style Classification

The variation in orthogonal layer thickness (t_α) at various inclinations (α) of the fold limbs in minor folds, which was found for twenty-four minor folds, the (t'_α) and (α) diagram defined fold types within both anticlines, indicating that these minor folds mainly match with parallel fold subclass 1B and a tendency towards class 2. Appendix (B) and Figure 7 contain details.

The relationship between the aspect ratio ($h = y_0/x_0$) and the normalized area ($A = 2A/x_0y_0$) reveals changes in the outer and inner arcs of each limb. This was determined by analyzing eighteen minor folds from both anticlines. The classification of the shapes of the single-folded surfaces shows transitional shapes that range from an ellipse shape to a chevron shape, shown in Figure 9. The diagram displaying aspect ratio against normalized area provides the basis for this classification; details are included in Appendix (C) and Figure 8.

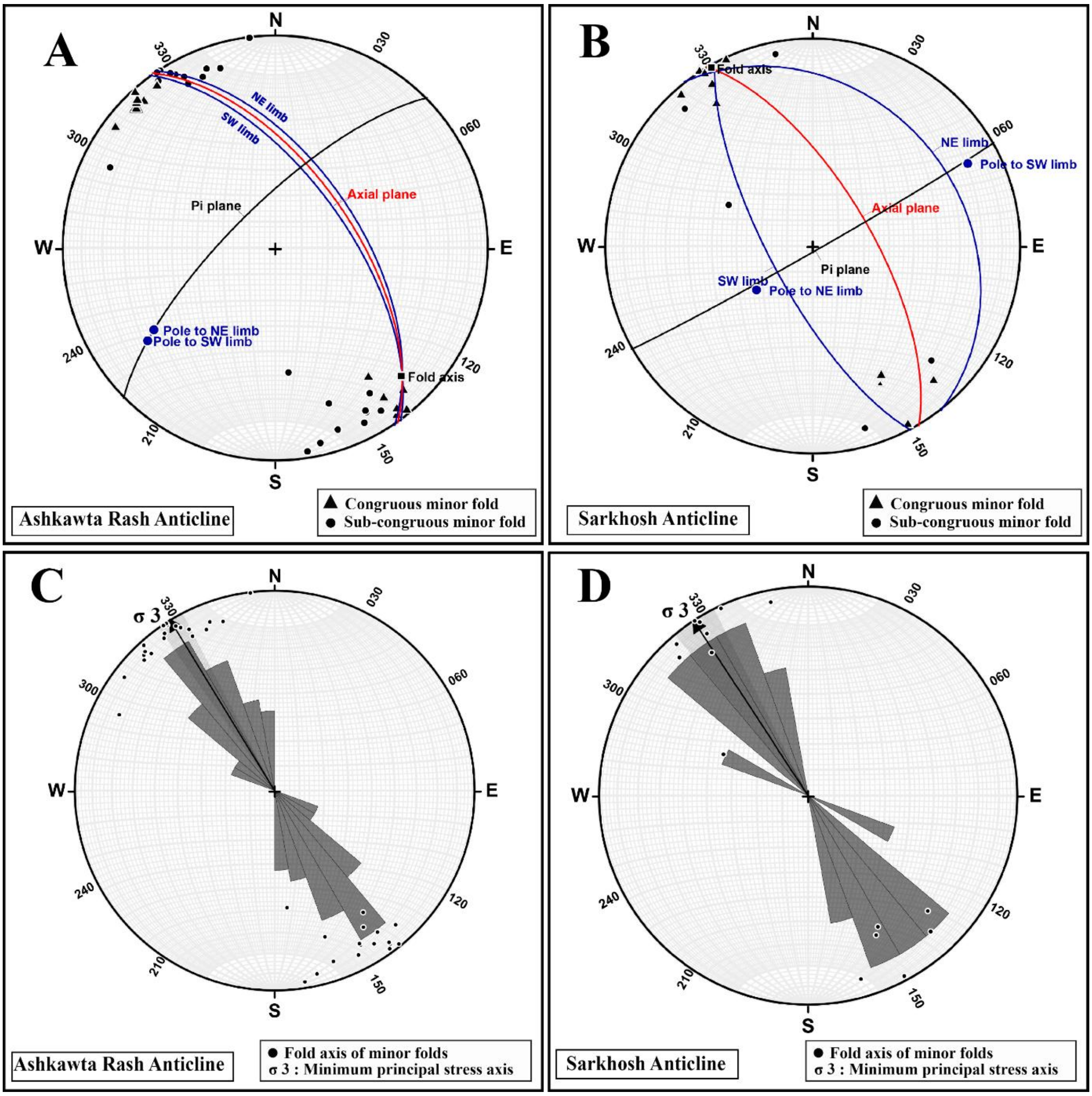

Figure 6. (A) and (B) are stereographic projections that illustrate the minor folds in Ashkawta Rash and Sarkhosh anticlines, and they also show the distribution of directions of the axes of the minor folds in relation to the axis of the major fold. (C) and (D) show the direction of the minimum principal stress axis (σ_3) from the minor folds in both anticlines.

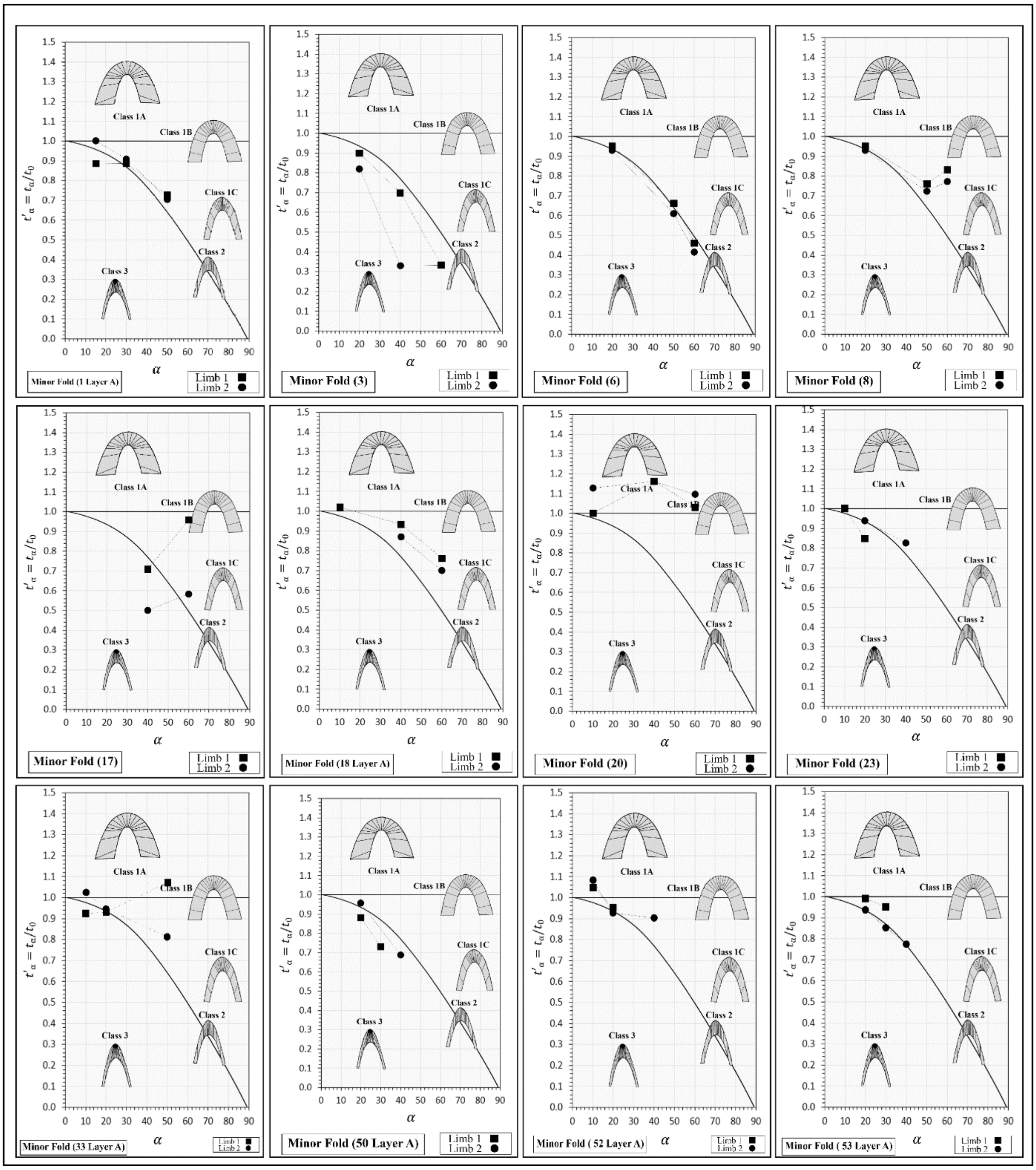

Figure 7. Minor fold types that are defined on the diagram are called (t'α) and (α).

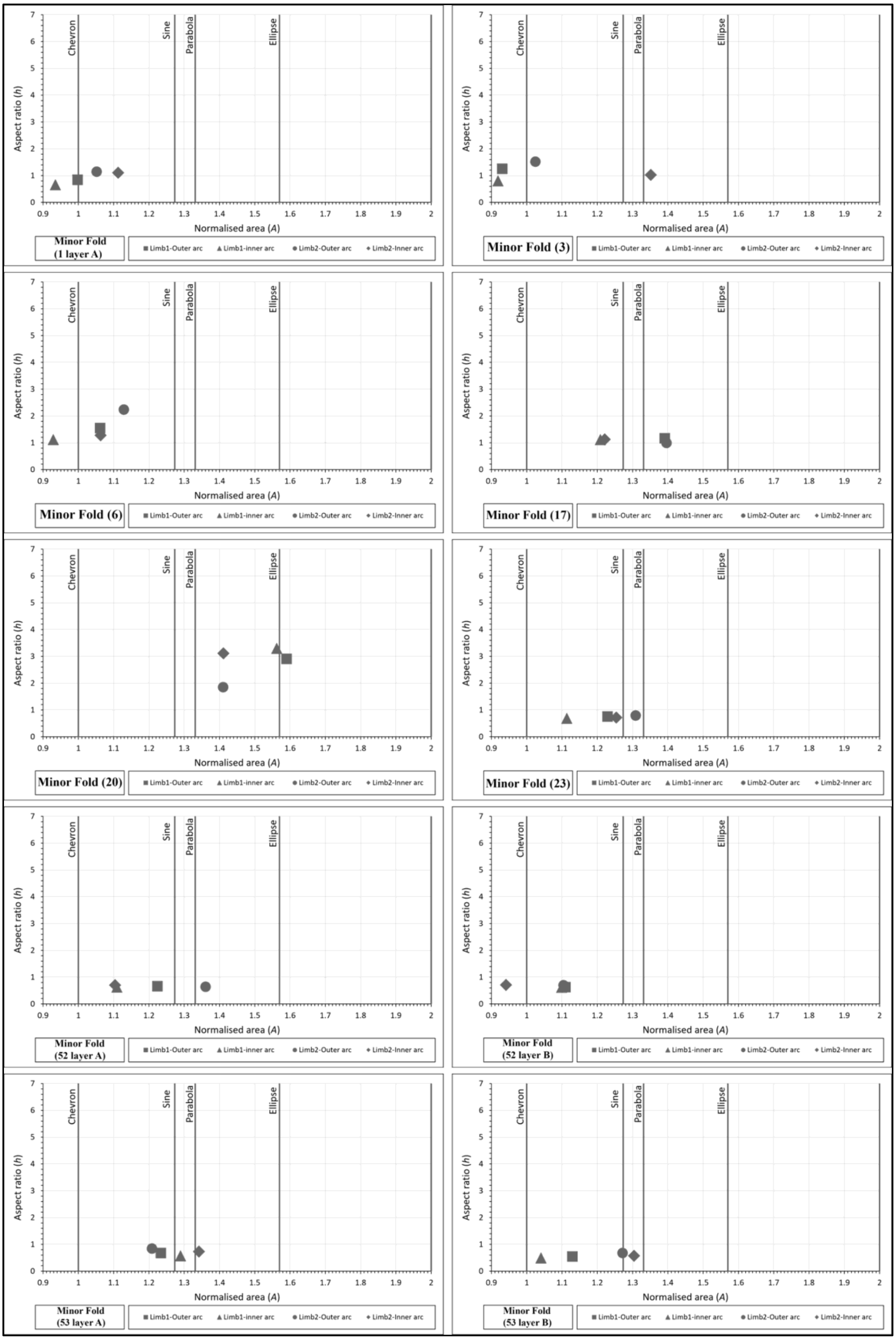

Figure 8. Based on the diagram of aspect ratio against normalized area, the minor fold is classified into different styles of single-folded surface styles.

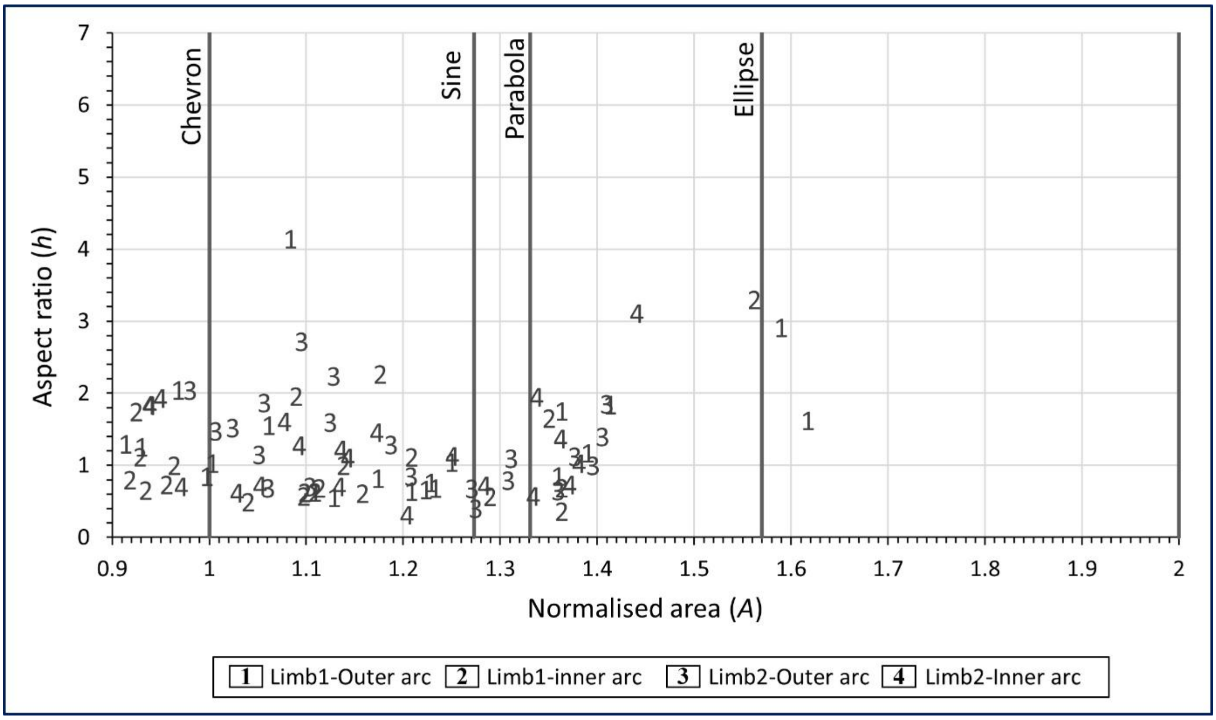

Figure 9. Eighteen minor folds in both anticline shapes, ranging from an ellipse shape to a chevron shape, based on the diagram that compares the normalized area to the aspect ratio.

5. Discussion

Part of the Alpine-Himalayan mountain range, the Zagros Orogenic Belt extends for about 2,000 km, starting in southeastern Turkey at the Anatolian Fault and ending in southern Iran at the Makran Zone (Al-Qayim et al., 2012). Historically, the collision of the Arabian and Eurasian plates has led to the development of the faults and folds of the Zagros fold-thrust belt (Abdulnaby, 2019). The study area occurs in the Zagros Imbricate Zone. This "Zagros Imbricate Zone" is bordered to the southwest by the High Zagros Reverse Fault and to the northeast by the Zagros Thrust Front. The sedimentary succession of this zone is composed of parautochthonous plate margin deposits, which include the Balambo Formation, which contains Cretaceous marine carbonates, the Tanjero Formation, which is representative of the Late Cretaceous foreland flysch, and the Suwais Red Bed, which is the Paleogene foreland molasse sequence (Al-Qayim et al., 2012). The zone is heavily deformed and markedly shorter relative to the other layers of the Arabian border. Deformation occurred through shortening caused by the displacement of the suture zone masses and the following collision event. Imbrications appear in the structural style, marked by tight, overturned, high-amplitude, dense folds associated with extensive faulting (Al-Qayim et al., 2012; Fouad, 2015). The Ashkawta Rash and Sarkhosh anticlines follow the general Zagros fold trend NW – SE. The fold axis orientations of the 24 congruous minor folds determined are simultaneously formed by the same stress state as the major folds, Figure 6C and D. The oblique collision and anticlockwise rotation of Arabia relative to the Eurasian plate may have caused subsequent stress phases that eventually developed the sub-congruous minor folds with axes that diverge from the axis of the major structure, which range from 296° to 354° (Abdullah et al., 2023; Abdulnaby et al., 2014; Aswad, 1999; Numan, 1997; Numan, 2001).

Buckling and flattening mechanisms cause the development of minor folds, revealed by the geometric analysis of fold styles and classifications of single-fold surfaces. The buckling mechanism is the principal process through which parallel folds (subclass 1B) develop when the folded layer has more competence than the matrix, according to (Hudleston, 1973; Ramsay & Huber, 1987). The flattening process when folds changed shape was induced by superimposed strain processes, resulting in limb thinning and geometries that were more consistent with those of similar folds. In addition, reference (Bastida et al., 2007; Srivastava & Shah, 2006; Zagorčev, 1993) indicates that flattening caused a geometric transition, modifying the folds from sub-class 1B to Class 1C morphology. According to the shape of the single-fold surface classification, the majority of minor folds have a sinusoidal shape, with a few revealing a chevron shape. Homogeneous flattening facilitates the shift from sinusoidal to chevron geometries, as the chevron shape is typically a similar fold or class 2. As detailed in (Al-Hakari, 2023), the investigation of the geometry of minor folds in the Qaiwan and Goizhah anticlines, adjacent to our research region, indicates that the mechanisms driving their development encompass both buckling and flattening, as determined by fold style classifications.

6. Conclusions

The geometrical and tectonic analysis of fifty-three minor folds in the Ashkawta Rash and Sarkhosh Anticlines, located within the Cretaceous succession of the Balambo and Kometan formations, reveals significant variation in fold development and geometries. The differences correspond to variations in lithology and the degree of folding deformation. Twenty-four minor folds are congruous, and twenty-nine are sub-congruous, depending on the orientation of the minor fold hinges and their association with the major folds. The congruous folds indicate production under a compressive stress state directed NE – SW, probably responsible for the initial folding. These folds may have formed while on the tightening phase of the major folds undergoing comparable change. The direction of the fold axes in the sub-congruous minor folds, ranging from 296° to 354°, can be attributed to the oblique collision and anticlockwise rotation of the Arabian Plate relative to the Eurasian Plate. This indicates that these tectonic processes were essential in the development of the sub-congruous folds. The geometric analysis of fold styles and classifications of single-fold surfaces suggests that the formation of minor folds is influenced by buckling and flattening mechanisms. Sub-class 1B parallel folds are mainly caused by buckling when the folded layer has greater competency compared to the surrounding matrix. Homogeneous flattening enables the transition of fold geometries from sinusoidal to chevron shapes, classifying chevron folds as similar folds or Class 2.

Appendix A. Geometric properties of the minor folds in the research location.

Ashkawta Rash Anticline Minor Folds										
Minor fold Number	Formation	Location in the major fold	Attitude of the minor fold		Fold axis	Axial plane	Interlimb angle	Relation to the major fold	Fleuty classification (Fleuty, 1964)	
			Limb 1	Limb 2					Based on the interlimb angle	Based on the axial plane dip and hinge plunge
1	Kometan	NE limb	308/52	142/54	315/09	315/89	74	Congruous	Open	Sub-vertical, Sub-horizontal
2	Kometan	NE limb	142/54	338/63	151/13	150/86	63	Sub-congruous	Close	Sub-vertical, Gently plunging
3	Kometan	NE limb	338/63	143/63	151/14	151/90	54	Sub-congruous	Close	Sub-vertical, Gently plunging
4	Kometan	NE limb	313/60	146/53	318/9	139/86	67	Congruous	Close	Sub-vertical, Sub-horizontal
5	Kometan	NE limb	146/53	335/74	153/09	151/80	53	Sub-congruous	Close	Sub-vertical, Sub-horizontal
6	Kometan	NE limb	335/74	148/62	153/09	152/84	44	Sub-congruous	Close	Sub-vertical, Sub-horizontal
7	Kometan	NE limb	148/62	327/85	327/02	148/79	33	Sub-congruous	Close	Steeply inclined, Sub-horizontal
8	Kometan	NE limb	327/85	149/26	327/01	148/61	69	Sub-congruous	Close	Steeply inclined, Sub-horizontal
9	Kometan	NE limb	323/47	154/58	330/07	329/85	75	Sub-congruous	Open	Sub-vertical, Sub-horizontal
10	Kometan	NE limb	325/85	175/10	325/05	149/52	85	Sub-congruous	Open	Moderately inclined, Sub-horizontal
11	Kometan	NE limb	175/10	135/44	307/07	143/26	36	Congruous	Close	Gently inclined, Sub-horizontal
12	Kometan	NE limb	313/64	151/25	316/07	139/70	91	Congruous	Open	Steeply inclined, Sub-horizontal
13	Kometan	NE limb	151/25	290/68	296/15	123/67	87	Sub-congruous	Open	Steeply inclined, Gently plunging
14	Kometan	NE limb	141/44	325/65	144/03	143/80	71	Congruous	Open	Sub-vertical, Sub-horizontal
15	Kometan	NE limb	325/65	138/43	143/05	142/79	72.3	Congruous	Open	Steeply inclined, Sub-horizontal
16	Kometan	SW limb	146/77	312/05	326/1	325/54	98.1	Sub-congruous	Open	Moderately inclined, Sub-horizontal
17	Kometan	SW limb	167/55	321/32	339/11	337/78	95.5	Sub-congruous	Open	Steeply inclined, Gently plunging

18	Kometan	SW limb	321/32	165/80	343/13	337/66	70.8	Sub-congruous	Close	Steeply inclined, Gently plunging
19	Kometan	SW limb	234/45	160/74	174/41	010/72	90.8	Sub-congruous	Open	Steeply inclined, Moderately plunging
20	Kometan	SW limb	329/72	156/68	332/10	153/88	41.1	Sub-congruous	Close	Sub-vertical, Gently plunging
21	Kometan	SW limb	351/18	173/72	353/01	353/63	90	Sub-congruous	Open	Steeply inclined, Sub-horizontal
22	Kometan	SW limb	353/32	160/78	162/07	345/67	70.8	Sub-congruous	Open	Steeply inclined, Sub-horizontal
23	Balambo	SW limb	353/42	155/64	161/11	343/79	75.7	Sub-congruous	Open	Steeply inclined, Gently plunging
24	Balambo	SW limb	353/64	157/82	161/24	345/81	37.4	Sub-congruous	Close	Sub-vertical, Gently plunging
25	Kometan	NE limb	348/50	128/60	144/26	327/85	79.2	Congruous	Open	Sub-vertical, Gently plunging
26	Kometan	NE limb	333/58	139/70	144/14	326/84	53.7	Congruous	Close	Sub-vertical, Gently plunging
32	Kometan	NE limb	313/55	140/60	317/6	317/88	65.3	Congruous	Close	Sub-vertical, Sub-horizontal
33	Kometan	NE limb	140/60	311/24	318/3	317/72	96.2	Congruous	Open	Steeply inclined, Sub-horizontal
34	Kometan	NE limb	140/60	136/24	141/2	139/42	36.1	Congruous	Close	Moderately inclined, Sub-horizontal
35	Kometan	NE limb	136/62	331/80	147/20	144/81	40.7	Sub-congruous	Close	Sub-vertical, Gently plunging
36	Kometan	NE limb	326/59	137/46	143/06	142/84	75.4	Congruous	Open	Sub-vertical, Sub-horizontal
37	Kometan	NE limb	137/46	330/72	147/10	144/77	63.1	Sub-congruous	Close	Steeply inclined, Gently plunging
45	Balambo	Hinge	185/28	306/26	337/14	337/89	133.4	Sub-congruous	Gentle	Sub-vertical, Gently plunging
49	Kometan	SW limb	131/60	325/56	138/11	318/88	65.4	Congruous	Close	Sub-vertical, Gently plunging
50	Kometan	NE limb	167/50	357/33	171/04	351/82	97.4	Sub-congruous	Open	Sub-vertical, Sub-horizontal
51	Kometan	NE limb	153/54	327/65	329/05	150/85	61.3	Sub-congruous	Close	Sub-vertical, Sub-horizontal
52	Kometan	NE limb	161/58	320/49	332/14	331/85	75.5	Sub-congruous	Open	Sub-vertical, Gently plunging
53	Kometan	NE limb	320/59	146/78	324/07	323/81	43.4	Congruous	Close	Sub-vertical, Sub-horizontal

Sarkhosh Anticline Minor Folds

Minor fold Number	Formation	Location in the major fold	Attitude of the minor fold		Fold axis	Axial plane	Interlimb angle	Relation to the major fold	Fleuty classification(Fleuty, 1964)	
			Limb 1	Limb 2					Based on the interlimb angle	Based on the axial plane dip and hinge plunge
27	Balambo	Hinge	345/81	152/40	164/10	160/69	60.1	Sub-congruous	Close	Steeply inclined, Gently plunging
28	Balambo	Hinge	317/66	151/24	319/05	141/69	90.6	Congruous	Open	Steeply inclined, Sub-horizontal
29	Balambo	Hinge	176/20	153/61	328/10	159/40	43	Congruous	Close	Moderately inclined, Gently plunging
30	Balambo	Hinge	176/18	305/44	317/11	140/76	124.4	Sub-congruous	Gentle	Steeply inclined, Gently plunging
31	Balambo	Hinge	305/44	166/45	326/19	146/90	97	Congruous	Open	Vertical, Gently plunging
38	Balambo	NE limb	156/08	326/42	327/01	148/73	130.1	Congruous	Gentle	Steeply inclined, Sub-horizontal
39	Balambo	NE limb	140/70	343/72	152/30	152/89	44.2	Congruous	Close	Sub-vertical, Moderately plunging
40	Balambo	NE limb	343/72	137/60	154/27	151/84	54.1	Congruous	Close	Sub-vertical, Gently plunging
41	Balambo	NE limb	175/48	342/48	349/07	169/90	84.8	Sub-congruous	Open	Vertical, Sub-horizontal
42	Balambo	NE limb	130/80	155/65	296/53	142/72	28.1	Sub-congruous	Tight	Steeply inclined, Moderately plunging
43	Balambo	NE limb	110/45	338/45	134/22	134/90	99.5	Sub-congruous	Open	Vertical, Gently plunging
44	Balambo	NE limb	131/65	320/80	138/14	136/83	36.1	Congruous	Close	Sub-vertical, Gently plunging
46	Balambo	NE limb	159/19	334/65	335/02	155/67	96.1	Congruous	Open	Steeply inclined, Sub-horizontal
47	Balambo	NE limb	334/48	147/31	152/03	151/82	101.2	Congruous	Open	Sub-vertical, Sub-horizontal
48	Balambo	NE limb	155/23	323/35	328/03	148/84	122.3	Congruous	Gentle	Sub-vertical, Sub-horizontal

Appendix B. Calculation elements for the style of folded layers for minor folds, as described by Ramsay & Huber (1987).

Minor fold Number	Limb 1					Limb 2				
	α	t_α (m)	t_0 (m)	$t'_\alpha = t_\alpha/t_0$	Class	α	t_α (m)	t_0 (m)	$t'_\alpha = t_\alpha/t_0$	Class
1 Layer A	15	0.39	0.44	0.886	2 to 1C	15	0.44	0.44	1.000	1B to 1C
	30	0.39	0.44	0.886		30	0.4	0.44	0.909	
	50	0.32	0.44	0.727		50	0.31	0.44	0.705	
1 Layer B	40	0.25	0.31	0.806	1A to 2	40	0.17	0.31	0.548	2 to 1C
	60	0.39	0.31	1.258		60	0.16	0.31	0.516	
3	20	0.30	0.33	0.909	3	20	0.27	0.33	0.818	3
	40	0.23	0.33	0.697		40	0.11	0.33	0.333	
	60	0.11	0.33	0.333		60	0.11	0.33	0.333	
4	10	0.55	0.59	0.932	3	10	0.58	0.59	0.983	2
	20	0.47	0.59	0.797		20	0.54	0.59	0.915	
	50	0.18	0.59	0.305		50	0.25	0.59	0.424	
6	20	0.39	0.41	0.951	2	20	0.38	0.41	0.927	2
	50	0.27	0.41	0.659		50	0.25	0.41	0.610	
	60	0.19	0.41	0.463		60	0.17	0.41	0.415	
8	20	0.78	0.82	0.951	2 to 1C	20	0.76	0.82	0.927	2 to 1C
	50	0.62	0.82	0.756		50	0.59	0.82	0.720	
	60	0.68	0.82	0.829		60	0.63	0.82	0.768	
16	30	0.06	0.07	0.857	2 to 1C	30	0.07	0.07	1.000	1B
	60	0.06	0.07	0.857		60	0.07	0.07	1.000	
17	40	0.17	0.24	0.708	1C to 2	40	0.12	0.24	0.500	1C
	60	0.23	0.24	0.958		60	0.14	0.24	0.583	
18 Layer A	10	0.47	0.46	1.022	1B to 1C	40	0.4	0.46	0.870	1B to 1C
	40	0.43	0.46	0.935		60	0.32	0.46	0.696	
	60	0.35	0.46	0.761						
18 Layer B	20	0.65	0.53	1.226	1A to 1C	20	0.64	0.53	1.208	1A to 1B
	30	0.58	0.53	1.094		50	0.52	0.53	0.981	
	50	0.44	0.53	0.830						
19	30	1.12	1.27	0.882	2 to 1C	30	1.07	1.27	0.843	2
	40	1.06	1.27	0.835		40	0.95	1.27	0.748	
20	10	0.31	0.31	1.000	1B	10	0.35	0.31	1.129	1A
	40	0.36	0.31	1.161		40	0.36	0.31	1.161	
	60	0.32	0.31	1.032		60	0.34	0.31	1.097	
22	20	0.41	0.44	0.932	2 to 1C	20	0.45	0.44	1.023	1B to 1C
	50	0.27	0.44	0.614		50	0.39	0.44	0.886	
	60	0.28	0.44	0.636		60	0.32	0.44	0.727	
23	10	1.32	1.32	1.000	1B	20	1.24	1.32	0.939	2 to 1C
	20	1.12	1.32	0.848		40	1.09	1.32	0.826	
24	20	0.47	0.47	1.000	1B to 1C	20	0.43	0.47	0.915	2
	40	0.43	0.47	0.915		40	0.36	0.47	0.766	
	60	0.3	0.47	0.638		60	0.19	0.47	0.404	

26 Layer A	40	0.21	0.25	0.840	1C	40	0.23	0.25	0.920	1C
	60	0.18	0.25	0.720		60	0.14	0.25	0.560	
26 Layer B	40	0.62	0.79	0.785	2	40	0.61	0.79	0.772	2
	60	0.44	0.79	0.557		60	0.43	0.79	0.544	
	10	0.7	0.76	0.921		10	0.78	0.76	1.026	
33 Layer A	20	0.71	0.76	0.934	1B to 2	20	0.72	0.76	0.947	1B to C
	50	0.81	0.76	1.066		50	0.62	0.76	0.816	
	10	0.5	0.61	0.820		10	0.63	0.61	1.033	
33 Layer B	20	0.74	0.61	1.213	1A to 1C	20	0.62	0.61	1.016	1B to 2
	50	0.44	0.61	0.721		50	0.39	0.61	0.639	
34 Layer A	20	0.54	0.44	1.227	1B	20	0.47	0.44	1.068	1A
	30	0.61	0.44	1.386		30	0.45	0.44	1.023	
	20	0.29	0.28	1.036		10	0.21	0.28	0.750	
34 Layer B	30	0.3	0.28	1.071	1B to 2	30	0.22	0.28	0.786	3
	40	0.21	0.28	0.750		40	0.19	0.28	0.679	
	10	0.65	0.66	0.985		10	0.71	0.66	1.076	
39	30	0.7	0.66	1.061	1B to 1C	30	0.72	0.66	1.091	1C
	50	0.61	0.66	0.924		50	0.55	0.66	0.833	
	10	0.75	0.76	0.987		10	0.67	0.76	0.882	
41	20	0.78	0.76	1.026	1B	20	0.64	0.76	0.842	1B
	40	0.73	0.76	0.961		40	0.75	0.76	0.987	
	10	0.27	0.25	1.080		20	0.28	0.25	1.120	
42	20	0.21	0.25	0.840	1A to 3	30	0.22	0.25	0.880	1A -1C
						50	0.2	0.25	0.800	
	10	0.12	0.13	0.923		10	0.12	0.13	0.923	
46	30	0.13	0.13	1.000	1B	30	0.12	0.13	0.923	1C
						50	0.1	0.13	0.769	
47	10	0.16	0.15	1.067	1A to 3	10	0.15	0.15	1.000	1B
	20	0.13	0.15	0.867		20	0.13	0.15	0.867	
50 Layer A	20	0.82	0.93	0.882	3	20	0.89	0.93	0.957	1B to 1C
	30	0.68	0.93	0.731		40	0.64	0.93	0.688	
	20	0.58	0.63	0.921		20	0.57	0.63	0.905	2
50 Layer B	30	0.58	0.63	0.921	2 to 1C	40	0.43	0.63	0.683	
	40	0.4	0.63	0.635						
52 Layer A	10	0.87	0.83	1.048	1B to 1C	10	0.9	0.83	1.084	1B to 1C
	20	0.79	0.83	0.952		20	0.77	0.83	0.928	
						40	0.75	0.83	0.904	
	20	1.28	1.29	0.992		20	1.21	1.29	0.938	
53 Layer A	30	1.23	1.29	0.953	1B to 1C	30	1.1	1.29	0.853	2
						40	1	1.29	0.775	

Appendix C. Calculation parameters for asymmetrically shaped folded surfaces related to the classification of minor folds according to (Bastida et al., 1999; Bastida et al., 2005).

		limb 1						limb 2					
Minor fold Number	**Layer and Limb**	**A, area beneath the limb profile (m2)**	**X0 (m)**	**Y0 (m)**	**Aspect ratio, h=y0/x0**	**Normalised area (A=2A/x0y0)**	**Classification**	**A, area beneath the limb profile (m2)**	**X0 (m)**	**Y0 (m)**	**Aspect ratio, h=y0/x0**	**Normalised area (A=2A/x0y0)**	**Classification**
1	Layer A-Outer arc	0.264	0.79	0.67	0.848	0.998	Chevron	0.68	1.06	1.22	1.151	1.052	Sine
	Layer A-Inner arc	0.103	0.58	0.38	0.655	0.935	Chevron	0.533	0.93	1.03	1.108	1.113	Sine
	Layer B-Outer arc	0.317	0.74	0.63	0.851	1.360	Ellipse	0.246	0.5	0.7	1.400	1.406	Ellipse
	Layer B-Inner arc	0.071	0.45	0.33	0.733	0.956	Chevron	0.069	0.32	0.39	1.219	1.106	Sine
2	Outer arc	0.011	0.07	0.29	4.143	1.084	Sine	0.053	0.23	0.47	2.043	0.981	Chevron
	Inner arc	0.012	0.16	0.11	0.688	1.364	Ellipse	0.023	0.25	0.18	0.720	1.022	Sine
3	Outer arc	0.108	0.43	0.54	1.256	0.930	Chevron	0.151	0.44	0.67	1.523	1.024	Sine
	Inner arc	0.045	0.35	0.28	0.800	0.918	Chevron	0.09	0.36	0.37	1.028	1.351	Ellipse
4	Outer arc	0.128	0.46	0.48	1.043	1.159	Sine	0.145	0.45	0.58	1.289	1.111	Sine
	Inner arc	0.102	0.46	0.46	1.000	0.964	Chevron	0.075	0.3	0.55	1.833	0.909	Chevron
5	Outer arc	0.131	0.47	0.61	1.298	0.914	Chevron	0.144	0.44	0.65	1.477	1.007	Chevron
	Inner arc	0.003	0.11	0.04	0.364	1.364	Ellipse	0.048	0.24	0.35	1.458	1.143	Sine
6	Outer arc	0.107	0.36	0.56	1.556	1.062	Sine	0.079	0.25	0.56	2.240	1.129	Sine
	Inner arc	0.015	0.17	0.19	1.118	0.929	Chevron	0.022	0.18	0.23	1.278	1.063	Sine
8	Outer arc	0.789	1.28	1.05	0.820	1.174	Sine	0.714	0.96	1.08	1.125	1.377	Ellipse
	Inner arc	0.962	1.3	1.3	1.000	1.138	Sine	0.169	0.43	0.59	1.372	1.332	Parabola
10	Outer arc	0.527	1.01	1.04	1.030	1.003	Chevron	0.689	0.68	1.85	2.721	1.095	Sine
	Inner arc	0.177	0.75	0.43	0.573	1.098	Sine	0.051	0.2	0.39	1.950	1.308	Parabola

16	Outer arc	0.047	0.19	0.35	1.842	1.414	Ellipse	0.036	0.2	0.32	1.600	1.125	Sine
	Inner arc	0.03	0.15	0.34	2.267	1.176	Sine	0.02	0.15	0.29	1.933	0.920	Chevron
17	Outer arc	1.097	1.16	1.36	1.172	1.391	Ellipse	0.578	0.91	0.91	1.000	1.396	Ellipse
	Inner arc	0.499	0.86	0.96	1.116	1.209	Sine	0.146	0.46	0.52	1.130	1.221	Sine
20	Outer arc	0.49	0.46	1.34	2.913	1.590	Box	0.486	0.61	1.13	1.852	1.410	Ellipse
	Inner arc	0.232	0.3	0.99	3.300	1.562	Ellipse	0.16	0.27	0.84	3.111	1.411	Ellipse
22	Outer arc	0.637	0.73	1.28	1.753	1.363	Ellipse	0.121	0.41	0.45	1.098	1.312	Parabola
	Inner arc	0.267	0.5	0.98	1.960	1.090	Sine	0.066	0.28	0.45	1.607	1.048	Sine
23	Outer arc	0.516	1.05	0.8	0.762	1.229	Sine	0.76	1.21	0.96	0.793	1.309	Parabola
	Inner arc	0.421	1.05	0.72	0.686	1.114	Sine	0.489	1.04	0.75	0.721	1.254	Sine
24	Outer arc	0.625	0.69	1.12	1.623	1.617	Box	0.251	0.83	0.57	0.687	1.061	Sine
	Inner arc	0.302	0.52	0.86	1.654	1.351	Ellipse	0.156	0.71	0.44	0.620	0.999	Chevron
40	Outer arc	1.751	1.33	2.72	2.045	0.968	Chevron	1.91	1.39	2.6	1.871	1.057	Sine
	Inner arc	0.775	0.98	1.71	1.745	0.925	Chevron	0.722	0.93	1.71	1.839	0.908	Chevron
41	Outer arc	4.479	3.4	2.18	0.641	1.209	Sine	1.581	2.48	1	0.403	1.275	Sine
	Inner arc	2.799	2.81	1.72	0.612	1.158	Sine	0.895	2.21	0.69	0.312	1.174	Sine
52	Layer A- Outer arc	2.418	2.44	1.62	0.664	1.223	Sine	3.74	2.91	1.89	0.649	1.360	Ellipse
	Layer A- Inner arc	1.829	2.29	1.44	0.629	1.109	Sine	2.883	2.72	1.92	0.706	1.104	Sine
	Layer B- Outer arc	1.829	2.29	1.44	0.629	1.109	Sine	2.883	2.72	1.92	0.706	1.104	Sine
	Layer B- Inner arc	2.667	2.79	1.74	0.624	1.099	Sine	2.935	2.97	2.1	0.707	0.941	Chevron
53	Layer A- Outer arc	2.636	2.5	1.71	0.684	1.233	Sine	6.755	3.63	3.08	0.848	1.208	Sine
	Layer A- Inner arc	1.575	2.07	1.18	0.570	1.290	Parabola	4.275	2.95	2.16	0.732	1.342	Ellipse
	Layer B- Outer arc	1.016	1.8	1	0.556	1.129	Sine	2.574	2.44	1.66	0.680	1.271	Sine
	Layer B- Inner arc	0.593	1.52	0.75	0.493	1.040	Sine	1.528	2.02	1.16	0.574	1.304	Parabola

Acknowledgments

The authors sincerely thank Dr. Ghafor Ameen Hamasur from the Department of Earth Sciences and Petroleum, University of Sulaimani, for his important advice and support during the fieldwork. His knowledge and expertise in structural geology greatly increased our understanding of the studied area.

References

Abdullah, N. M., Al Sumaidaie, M. A., & Aljumaily, I. S. (2023). Extrapolation Paleostress Orientations Deduced from Joints Analyses at Spi Rais and West Part of Chai Gara Anticlines, Duhok Area, Kurdistan Region, Iraq. *The Iraqi Geological Journal*, 324-345. https://doi.org/https://doi.org/10.46717/igj.56.2D.24ms-2023-10-30

Abdulnaby, W. (2019). Structural geology and neotectonics of Iraq, Northwest Zagros. In *Developments in structural geology and tectonics* (Vol. 3, pp. 53-73). Elsevier. https://doi.org/https://doi.org/10.1016/B978-0-12-815048-1.00004-4

Abdulnaby, W., Mahdi, H., Al-Shukri, H., & Numan, N. M. (2014). Stress patterns in Northern Iraq and surrounding regions from formal stress inversion of earthquake focal mechanism solutions. *Pure and Applied Geophysics*, *171*, 2137-2153. https://doi.org/https://doi.org/10.1007/s00024-014-0823-x

Al-Hakari, S. (2023). Tectonic Implication and Geometry of the Minor Folds in Qaiwan and Goizhah Anticlines, Northeast of Sulaimani District, Northeastern Iraq. *Geotectonics*, *57*(5), 648-666. https://doi.org/https://doi.org/10.1134/S0016852123050035

Al-Hakari, S. H. S. (2011). Geometric analysis and structural evolution of NW Sulaimani area, Kurdistan Region, Iraq. *Unpublished Ph. D. Thesis, University of Sulaimani*.

Al-Qayim, B., Omer, A., & Koyi, H. (2012). Tectonostratigraphic overview of the Zagros suture zone, Kurdistan region, Northeast Iraq. *GeoArabia*, *17*(4), 109-156. https://doi.org/https://doi.org/10.2113/geoarabia1704109

Alavi, M. (2004). Regional stratigraphy of the Zagros fold-thrust belt of Iran and its proforeland evolution. *American journal of Science*, *304*(1), 1-20.

Allmendinger, R. W. (2011). *Stereonet. version 11.6.1* Retrieved 11/7/2024 from https://www.rickallmendinger.net/stereonet

Aswad, K. J. (1999). Arc-continent collision in Northeastern Iraq as evidenced by Mawat and Penjwin Ophiolite Complexes. *Rafidain Journal of Sciences*, *10*, 51-61.

Awais, M., Ishaq, M., Akhtar, N., Haroon, M., & Khan, S. (2016). Mesoscopic structures can give insights to the Regional Ones–An example of Pumpelly's rule from a part of Kala-Chitta Range near Kahi Village, Nizampur, Khyber Pakhtunkhwa, Pakistan: an insight into Economic Geology. *International Journal of Economic and Environmental Geology*, 80-84.

Bastida, F., Aller, J., & Bobillo-Ares, N. (1999). Geometrical analysis of folded surfaces using simple functions. *Journal of Structural Geology*, *21*(7), 729-742. https://doi.org/https://doi.org/10.1016/S0191-8141(99)00079-6

Bastida, F., Aller, J., Bobillo-Ares, N. C., & Toimil, N. C. (2005). Fold geometry: a basis for their kinematical analysis. *Earth-Science Reviews*, *70*(1-2), 129-164. https://doi.org/https://doi.org/10.1016/j.earscirev.2004.11.006

Bastida, F., Aller, J., Toimil, N. C., Lisle, R. J., & Bobillo-Ares, N. (2007). Some considerations on the kinematics of chevron folds. *Journal of Structural Geology*, *29*(7), 1185-1200. https://doi.org/https://doi.org/10.1016/j.jsg.2007.03.010

Bhattacharya, A. R. (2022). *Structural Geology*. Springer International Publishing. https://books.google.iq/books?id=9PGGEAAAQBAJ

Billings, M. P. (1974). *Structural Geology*. Prentice-Hall of India. https://books.google.iq/books?id=NfNynQAACAAJ

Fleuty, M. (1964). The description of folds. *Proceedings of the Geologists' Association*, *75*(4), 461-492. https://doi.org/https://doi.org/10.1016/S0016-7878(64)80023-7

Fossen, H. (2010). *Structural Geology*. Cambridge University Press. https://books.google.iq/books?id=01PI5jhjiiQC

Fossen, H. (2016). *Structural Geology*. Cambridge University Press. https://books.google.iq/books?id=sGoDEAAAQBAJ

Fouad, S. F. (2015). Tectonic map of Iraq, scale 1: 1000 000, 2012. *Iraqi bulletin of geology and mining*, *11*(1), 1-7. https://doi.org/https://ibgm-iq.org/ibgm/index.php/ibgm/article/view/262

Frehner, M., & Schmid, T. (2016). Parasitic folds with wrong vergence: How pre-existing geometrical asymmetries can be inherited during multilayer buckle folding. *Journal of Structural Geology*, *87*, 19-29. https://doi.org/https://doi.org/10.1016/j.jsg.2016.04.004

Hudleston, P. (1973). Fold morphology and some geometrical implications of theories of fold development. *Tectonophysics*, *16*(1-2), 1-46. https://doi.org/https://doi.org/10.1016/0040-1951(73)90129-7

Hudleston, P. J., & Lan, L. (1993). Information from fold shapes. *Journal of Structural Geology*, *15*(3-5), 253-264. https://doi.org/https://doi.org/10.1016/0191-8141(93)90124-S

Jassim, S. Z., & Goff, J. C. (2006). *Geology of Iraq*. DOLIN, sro, distributed by the Geological Society of London.

Lisle, R. J., Martínez, J. F., Bobillo-Ares, N., Menéndez, O., Aller, J., & Bastida, F. (2006). FOLD PROFILER: A MATLAB®—based program for fold shape classification. *Computers & Geosciences*, *32*(1), 102-108. https://doi.org/https://doi.org/10.1016/j.cageo.2005.05.007

Majeed, J. H. (2023). *Structural Study Of Kewa Charmula Anticline, Sulaymaniyah Governorate, Kurdistan Region, NE Iraq*, Sulaimani. University of Sulaimani.

Nabavi, S. T., & Fossen, H. (2021). Fold geometry and folding–a review. *Earth-Science Reviews*, *222*, 103812. https://doi.org/https://doi.org/10.1016/j.earscirev.2021.103812

Numan, N. M. (1997). A plate tectonic scenario for the Phanerozoic succession in Iraq. *Iraqi Geological Journal*, *30*(2), 85-110.

Numan, N. M. (2001). Cretaceous and Tertiary Alpine subductional history in northern Iraq. *Iraqi Journal of Earth Science*, *1*(2), 59-74.

Omar, A. (2005). An integrated structural and tectonic study of the Bina Bawi-Safin-Bradost region in Iraqi Kurdistan. *Unpublished Ph. D. Thesis, Department of Geology, Salahaddin University, Erbil*.

Ramsay, D. M., & Sturt, B. A. (1973). An analysis of noncylindrical and incongruous fold pattern from the Eo-Cambrian rocks of söröy, northern Norway: I. Noncylindrical, incongruous and aberrant folding. *Tectonophysics*, *18*(1-2), 81-107. https://doi.org/https://doi.org/10.1016/0040-1951(73)90078-4

Ramsay, J. G. (1967). Folding and fracturing of rocks. *McGraw-Hill Book Company*, *568*.

Ramsay, J. G., & Huber, M. I. (1987). *The Techniques of Modern Structural Geology: Folds and Fractures. Vol. 2*. Academic Press. https://books.google.iq/books?id=sScIzwEACAAJ

Rasband, W. (1987). *ImageJ. Version 1.54g*. Retrieved 12/11/2024 from https://imagej.net/ij/

Rowland, S. M., Duebendorfer, E. M., & Schiefelbein, I. M. (2007). *Structural Analysis and Synthesis: A Laboratory Course in Structural Geology*. Wiley. https://books.google.iq/books?id=IWnmBEtmg2MC

Srivastava, D. C., & Shah, J. (2006). A rapid method for strain estimation from flattened parallel folds. *Journal of Structural Geology*, *28*(1), 1-8. https://doi.org/https://doi.org/10.1016/j.jsg.2005.09.001

Zagorčev, I. S. (1993). The geometrical classification of folds and distribution of fold types in natural rocks. *Journal of Structural Geology*, *15*(3-5), 243-251. https://doi.org/https://doi.org/10.1016/0191-8141(93)90123-R

About the authors

Peshraw S. M. Khalifa obtained a bachelor's degree in geology from the Department of Geology, College of Science, University of Sulaimani, in 2016. From 2016 to 2019, he worked as a mudlogger for an oil company, gaining expertise in many oil fields. In 2019, he became an assistant geologist in the Department of Earth Science and Petroleum at the University of Sulaimani. He is now pursuing an M.Sc. in Structural Geology.

e-mail: Peshraw.mohammedkhalifa@univsul.edu.iq

Dr. Salim Hassan Suleiman Al-Hakari obtained a bachelor’s degree from the University of Mosul in 1989 and a master’s degree from the same university in 1993 in the field of structural geology, in the subject of paleostress analysis. His first employment was as an assistant lecturer at the University of Sulaimani in 2004, and then he obtained a Ph.D. from the University of Sulaimani in 2011 in structural geology with a focus on the geometry of the folds surrounding Sulaymaniyah city. He is now an assistant professor in structural geology at the same university. He has conducted numerous research papers about paleostress analysis and the geometry of the folds.

e-mail: Salim.sulaiman@univsul.edu.iq